Pergamon

Int. J. Solids Structures Vol. 31, No. 15, pp. 2053–2070, 1994
Elsevier Science Ltd
Printed in Great Britain
0020–7683/94 $7.00 + .00

0020–7683(94)E0017–P

FRACTURE MECHANICS OF COMPOSITES WITH NONHOMOGENEOUS INTERPHASES AND NONDILUTE FIBER VOLUME FRACTIONS

VERNON T. BECHEL and AUTAR K. KAW
Department of Mechanical Engineering, University of South Florida, Tampa, FL 33620-5350, U.S.A.

(*Received* 9 *July* 1993; *in revised form* 16 *December* 1993)

Abstract—A linear elastic fracture mechanics model is developed for a periodic composite geometry with a single cracked layer under uniform longitudinal strain. The interface between the fiber and the matrix can be nonhomogeneous, homogeneous or perfect. Four fracture mechanics models are considered: (1) dilute fiber volume fraction composite with nonhomogeneous interphases; (2) periodic composite with nondilute fiber volume fraction; (3) periodic composite with irregular fiber spacing near a matrix layer; (4) hybrid composites with more than one type of fiber. The stress intensity factors at the crack tips and the interface stress fields are studied to understand the fracture mechanics of composites as a function of the relative elastic moduli of the fiber, the matrix and the interphase, and the global and local fiber volume fractions.

INTRODUCTION

The presence of more than one constituent in continuous fiber reinforced composites results in many possible mechanisms of fracture. Many micromechanical models of composites have been developed to understand these mechanisms. These models account for axisymmetric cracks (Pagano and Brown, 1993), a fiber crack in dilute fiber volume fraction composites (Gupta, 1973), periodic cracks in nondilute fiber volume fraction composites (Erdogan and Bakioglu, 1976), and cracks in composites with nonhomogeneous interphases (Delale and Erdogan, 1988; Erdogan *et al.*, 1991). The above list is not complete but only presents the wide variety of problems solved in the literature on the fracture mechanics of composites.

In this study, a planar fracture mechanics model has been developed for a composite with a single damaged fiber or matrix layer. The fiber and the matrix layers are approximated by infinitely long, homogeneous, isotropic strips of finite width. These strips can have dissimilar elastic properties and widths. The fiber–matrix interphase (Drzal, 1983) between the fiber and the matrix can be nonhomogeneous, homogeneous or perfect.

Four important problems in fracture mechanics of composites are studied using the model developed in this paper. These are:

Model 1: composites with nonhomogeneous interphases,
Model 2: composites with nondilute fiber volume fractions,
Model 3: composites with irregular fiber spacing,
Model 4: hybrid composites,

with an initially damaged layer under a uniform remote axial strain along the length of the fiber.

The stress intensity factors and the stress fields at the crack tips are studied for the above models to understand the fracture mechanics of composites as a function of the relative elastic moduli of the fiber, the matrix and the interphase, and the global and local fiber volume fractions.

Model 1: *composites with nonhomogeneous interphases*

In a fiber reinforced composite a separate region, labeled the interphase (Drzal, 1983), may exist between the pure fiber material and the bulk matrix material. The interphase is

important in the mechanics of a composite. The transverse strength and stiffness, the axial compressive strength and the fracture toughness of a composite are influenced by the interphase properties. Jayaram *et al.* (1993a, b) reviewed the elastic and thermal effects of interphases for undamaged composites, while Chamis (1974) and Cornie *et al.* (1991) studied the effect of interphases on the fracture toughness of a composite.

The interphase region has different properties from that of the fiber and the matrix. It may consist of multiple regions of chemically distinct phases (Drzal, 1986; Brennan, 1987) or its properties may vary as a function of position along its width (Sottos *et al.*, 1992). Both these types of interphases can be modeled in this study and will henceforth be called nonhomogeneous interphases.

Fracture mechanics models, which account for nonhomogeneous interphases, have previously been developed by Delale and Erdogan (1988), Erdogan *et al.* (1991) and Kaw *et al.* (1992). In the above studies, the elastic moduli of the interphase varied exponentially along its width. In this paper, the effect of a nonhomogeneous interphase on the fracture mechanics of a composite is studied. However, in this paper, unlike the above studies, the interphase elastic moduli may vary as any arbitrary piecewise continuous function along its width.

Model 2: *composites with nondilute fiber volume fractions*

The effect of nondilute fiber volume fractions has been mostly excluded in studying the fracture mechanics of composites. Often, micromechanical composite fracture problems are solved using techniques where a crack is assumed in a layer bonded to an infinite layer. This may approximate composites either with dilute fiber volume fractions (Gupta, 1973) or a self consistent geometry (Whitney and Brown, 1993; Mori and Tanaka, 1973). Models which do use nondilute fiber volume fractions, also assume periodic cracks (Erdogan and Bakioglu, 1976). The current model is used to study the fracture mechanics of a single damaged layer composite with a nondilute fiber volume fraction.

Model 3: *composites with irregular fiber spacing*

The processing techniques for fiber reinforced composites produce internal defects, such as microcracks and uneven fiber spacing. Some fibers get placed further from each other than the average fiber distance, while other fibers may be placed closer together.

Barsoum *et al.* (1992) tested ceramic matrix composite samples in a three point bend test and found that matrix cracks initiated at a lower stress as the local fiber spacing increased. The present analytical model is used for qualitatively studying the matrix crack initiation stress as a function of this local fiber spacing.

Model 4: *hybrid composites*

Hybrid composites with more than one fiber type are developed for better impact resistance, increased fracture toughness and lower cost (Summerscales and Short, 1978; Agarwal and Broutman, 1991).

The fracture of multi-fiber hybrid composites is studied using the model developed in this paper. In particular, the effects of the elastic modulus and the volume fraction of the hybrid fibers on the fracture mechanics of a single damaged layer composite are investigated.

FORMULATION AND SOLUTION

The geometry of the problem is shown in Fig. 1. The composite consists of $(2n-1)$ planar strips of infinite length but finite width which are perfectly bonded, isotropic and linearly elastic. The central layer of width $2h_1$, Young's modulus E_1, shear modulus, $\mu_1(=E_1[2(1+\nu_1)])$ and Poisson's ratio ν_1 approximates a damaged fiber or matrix region. The crack has a half-crack length of "a" and is symmetric about the x_1 and y axes. The crack may touch the interface of the cracked layer and the first undamaged layer. The remaining undamaged fibers, the interphases and the matrix are approximated by $(2n-2)$ infinite strips of width h_i. The Young's modulus, $E_i(x_i)$ and Poisson's ratio, $\nu_i(x_i)$ of each undamaged strip may follow any variation through its width.

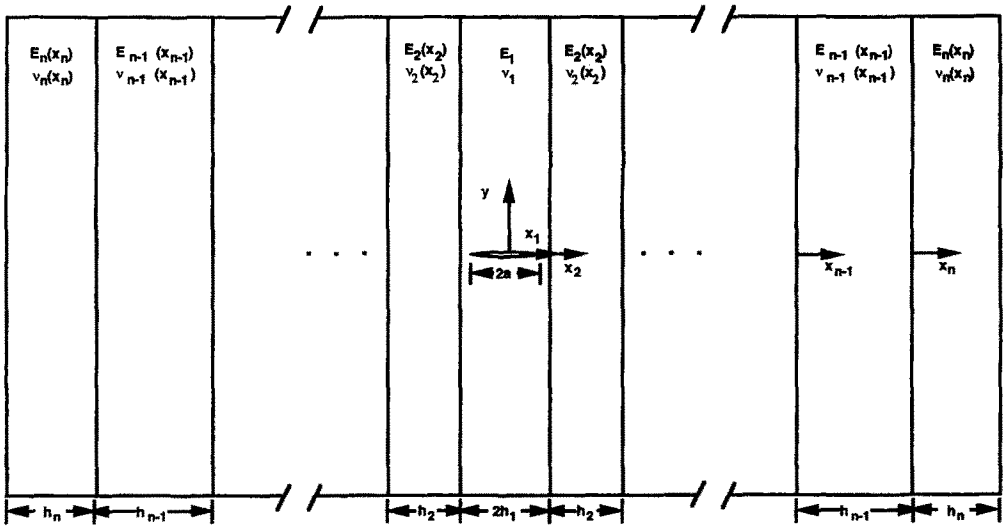

Fig. 1. Geometry of a composite with a single damaged layer.

The layered composite model is loaded with a remote uniform axial tensile strain, ε. Since the remote strain would cause a constant axial stress across each strip if no crack were present, superposition can be used to solve the problem. The overall solution is the sum of a problem with a damaged layer with a crack pressure of $p = E_1\varepsilon/(1-\nu_1^2)$ for plane strain and $p = E_1\varepsilon$ for plane stress, and an uncracked composite with a remote axial strain, ε. The uncracked problem has a simple solution. Therefore, only the pressurized crack problem is solved here.

Stress and displacement field equations

The displacement and stress field equations for a homogeneous infinitely long strip of finite width containing a symmetric crack aligned with the horizontal (x_1) axis are given (Gupta, 1973) as

$$u_1(x_1,y) = -\frac{2}{\pi}\int_0^\infty \left(\frac{1}{\eta}\left[f_1(\eta) - \frac{\kappa_1-1}{2}g_1(\eta)\right]\sinh(\eta x_1) + x_1 g_1(\eta)\cosh(\eta x_1)\right)\cos(\eta y)\,d\eta$$
$$-\frac{2}{\pi}\int_0^\infty \frac{\phi_1(\xi)}{\xi}\left(\frac{\kappa_1-1}{2} - \xi y\right)e^{-\xi y}\sin(\xi x_1)\,d\xi, \quad (1a)$$

$$v_1(x_1,y) = \frac{2}{\pi}\int_0^\infty \left(\frac{1}{\eta}\left[f_1(\eta) + \frac{\kappa_1+1}{2}g_1(\eta)\right]\cosh(\eta x_1) + x_1 g_1(\eta)\sinh(\eta x_1)\right)\sin(\eta y)\,d\eta$$
$$+\frac{2}{\pi}\int_0^\infty \frac{\phi_1(\xi)}{\xi}\left(\frac{\kappa_1+1}{2} + \xi y\right)e^{-\xi y}\cos(\xi x_1)\,d\xi, \quad (1b)$$

$$\sigma_{xx}^1(x_1,y) = -\frac{4\mu_1}{\pi}\int_0^\infty [f_1(\eta)\cosh(\eta x_1) + \eta x_1 g_1(\eta)\sinh(\eta x_1)]\cos(\eta y)\,d\eta$$
$$-\frac{4\mu_1}{\pi}\int_0^\infty \phi_1(\xi)(1-\xi y)e^{-\xi y}\cos(\xi x_1)\,d\xi, \quad (2a)$$

$$\sigma^1_{yy}(x_1,y)=\frac{4\mu_1}{\pi}\int_0^\infty([f_1(\eta)+2g_1(\eta)]\cosh(\eta x_1)+\eta x_1 g_1(\eta)\sinh(\eta x_1))\cos(\eta y)\,d\eta$$

$$-\frac{4\mu_1}{\pi}\int_0^\infty \phi_1(\xi)(1+\xi y)\,e^{-\xi y}\cos(\xi x_1)\,d\xi, \quad (2b)$$

$$\sigma^1_{xy}(x_1,y)=\frac{4\mu_1}{\pi}\int_0^\infty([f_1(\eta)+g_1(\eta)]\sinh(\eta x_1)+\eta x_1 g_1(\eta)\cosh(\eta x_1))\sin(\eta y)\,d\eta$$

$$-\frac{4\mu_1}{\pi}\int_0^\infty \xi y\phi_1(\xi)\,e^{-\xi y}\sin(\xi x_1)\,d\xi. \quad (2c)$$

The displacement and stress field equations for the ith nonhomogeneous infinite strip [Young's modulus and Poisson's ratio varying exponentially through the width $(E_i(x_i)=E_0^i e^{\beta_i x_i}, v_i(x_i)=(a_0^i+b_0^i x_i)e^{\beta_i x_i})$], are given (Delale and Erdogan, 1988; Kaw *et al.*, 1992):

$$u_i(x_i,y)=\frac{2}{\pi E_0^i}\int_0^\infty\left(\frac{\eta^2}{2}\left(\left[\frac{c_2^i(\eta)x_i}{m_2^i}+\frac{c_2^i(\eta)}{(m_2^i)^2}+\frac{c_1^i(\eta)}{m_2^i}\right]e^{-m_2^i x_i}\right.\right.$$

$$\left.+\left[\frac{c_4^i(\eta)x_i}{m_1^i}+\frac{c_4^i(\eta)}{(m_1^i)^2}+\frac{c_3^i(\eta)}{m_1^i}\right]e^{-m_1^i x_i}\right)$$

$$-[b_0^i c_2^i(\eta)m_1^i x_i^2+m_1^i x_i(a_0^i c_2^i(\eta)+b_0^i c_1^i(\eta))$$

$$+a_0^i c_1^i(\eta)m_1^i-b_0^i c_1^i(\eta)+a_0^i c_2^i(\eta)]\frac{e^{m_1^i x_i}}{2}$$

$$-[b_0^i c_4^i(\eta)m_2^i x_i^2+m_2^i x_i(a_0^i c_4^i(\eta)+b_0^i c_3^i(\eta))$$

$$\left.+a_0^i c_3^i(\eta)m_2^i-b_0^i c_3^i(\eta)+a_0^i c_4^i(\eta)]\frac{e^{m_2^i x_i}}{2}\right)\cos(\eta y)\,d\eta, \quad (3a)$$

$$v_i(x_i,y)=\frac{2}{\pi E_0^i}\int_0^\infty\left(\frac{1}{\eta}[((m_1^i)^2(c_1^i(\eta)+c_2^i(\eta)x_i)\right.$$

$$2m_1^i c_2^i(\eta))\,e^{-m_2^i x_i}+((m_2^i)^2(c_3^i(\eta)+c_4^i(\eta)x_i)$$

$$+2m_2^i c_4^i(\eta))\,e^{-m_1^i x_i}]+(a_0^i+b_0^i x_i)\eta[(c_1^i(\eta)$$

$$\left.+c_2^i(\eta)x_i)\,e^{m_1^i x_i}+(c_3^i(\eta)+c_4^i(\eta)x_i)\,e^{m_2^i x_i}]\right)\frac{\sin(\eta y)}{2}\,d\eta, \quad (3b)$$

$$\sigma^i_{xx}(x_i,y)=\frac{-2}{\pi}\int_0^\infty\frac{\eta^2}{2}[(c_1^i(\eta)+c_2^i(\eta)x_i)\,e^{m_1^i x_i}+(c_3^i(\eta)+c_4^i(\eta)x_i)\,e^{m_2^i x_i}]\cos(\eta y)\,d\eta, \quad (4a)$$

$$\sigma^i_{yy}(x_i,y)=\frac{2}{\pi}\int_0^\infty\frac{1}{2}([(m_1^i)^2(c_1^i(\eta)+c_2^i(\eta)x_i)+2m_1^i c_2^i(\eta)]\,e^{m_1^i x_i}+[(m_2^i)^2(c_3^i(\eta)$$

$$+c_4^i(\eta)x_i)+2m_2^i c_4^i(\eta)]\,e^{m_2^i x_i})\cos(\eta y)\,d\eta, \quad (4b)$$

$$\sigma^i_{xy}(x_i,y)=\frac{2}{\pi}\int_0^\infty\frac{\eta}{2}([m_1^i(c_1^i(\eta)+c_2^i(\eta)x_i)+c_2^i(\eta)]\,e^{m_1^i x_i}$$

$$+[m_2^i(c_3^i(\eta)+c_4^i(\eta)x_i)+c_4^i(\eta)]\,e^{m_2^i x_i})\sin(\eta y)\,d\eta, \quad (4c)$$

where

$$m_1^i = \frac{\beta_i}{2} - \left(\eta^2 + \frac{\beta_i^2}{4}\right)^{1/2}, \qquad m_2^i = \frac{\beta_i}{2} + \left(\eta^2 + \frac{\beta_i^2}{4}\right)^{1/2} \tag{5a, b}$$

E_0^i, β_i, a_0^i and b_0^i are four constants found from the Young's modulus and Poisson's ratio at the two edges ($x_i = 0$ and $x_i = h_i$) of the nonhomogeneous strip.

The stress and displacement fields for the nonhomogeneous strips can also be used for a homogeneous strip by allowing $b_0^i = \beta_i = 0$.

Boundary and continuity conditions

The continuity and boundary conditions are applied to the above stress and displacement equations to find the solution. The continuity conditions at the interfaces of each strip are given by

$$\sigma_{xx}^i(h_i, y) = \sigma_{xx}^{i+1}(0, y), \tag{6a}$$

$$\sigma_{xy}^i(h_i, y) = \sigma_{xy}^{i+1}(0, y), \tag{6b}$$

$$u_i(h_i, y) = u_{i+1}(0, y), \tag{6c}$$

$$v_i(h_i, y) = v_{i+1}(0, y), \tag{6d}$$

where $i = 1, 2, 3, \ldots (n-1)$, and $(2n-1)$ is the number of strips. Since the problem is symmetric, only the upper right quarter of the geometry was considered where $(n-1)$ strips are bonded to the right of the cracked layer.

The free edge boundary conditions on the outer layer n are

$$\sigma_{xx}^n(h_n, y) = 0, \tag{7a}$$

$$\sigma_{xy}^n(h_n, y) = 0. \tag{7b}$$

Finally, mixed boundary conditions at $y = 0$ in the cracked layer are given by

$$\sigma_{yy}^1(x_1, 0) = -p, \quad |x_1| < a, \tag{8a}$$

$$v_1(x_1, 0) = 0, \qquad a < |x_1| < h_1, \tag{8b}$$

$$v_i(x_i, 0) = 0, \qquad 0 < x_i < h_i, \quad i = 2, 3, \ldots, n. \tag{8c}$$

The condition of $\sigma_{xy}^i(x_i, 0) = 0$ is automatically satisfied for all the strips by eqns (2c) and (4c).

Derivation of the solution

The function $\phi_1(\xi)$ can be rewrittten in terms of the slope of the crack opening displacement, $[G(t) = \mathrm{d}v_1(t, 0)/\mathrm{d}t]$ as

$$\phi_1(\xi) = \frac{-2}{\kappa_1 + 1} \int_0^a G(t) \sin(\xi t)\, \mathrm{d}t. \tag{9}$$

There are now a total of $(4n-1)$ unknown functions, namely the three unknown functions f_1, g_1, $G(t)$ [instead of $\phi_1(\xi)$] from the central damaged strip and $(4n-1)$ unknown functions, $C_{1\text{-}4}^i$ from the other $(n-1)$ strips [see eqns (1)–(4)]. There are $(4n-2)$ boundary and continuity conditions given by eqns (6) and (7). These $(4n-2)$ conditions then allow $(4n-2)$ unknowns to be written in terms of only one unknown in a matrix form as

$$[\mathrm{A}][\mathrm{B}] = [\mathrm{C}]. \tag{10}$$

The coefficient matrix [A] of order $(4n-2) \times (4n-2)$ contains functions of x_i, t and n,

[B] is a vector of order $(4n-2)$ of the unknown functions excluding $G(t)$. The right hand side vector [C] of order $(4n-2)$ contains only integrals of $G(t)$ of the form

$$C_j = \int_{-a}^{a} G(t)h_j(t,\eta)\,dt, \quad 0 < \eta < \infty. \tag{11}$$

The above system of equations is solved implicity for f_1 and g_1 in terms of the integrals of $G(t)$. Substituting these implicit expressions in the remaining mixed boundary condition [eqn (8a)] gives

$$\int_{-a}^{a} \frac{G(t)}{t-x_1}\,dt + \int_{-a}^{a} G(t)K(t,x_1)\,dt = \frac{-\pi p(1+\kappa_1)}{4\mu_1}, \quad -a < x_1 < a. \tag{12}$$

Equation (12) is a Cauchy principal singular integral equation. The numerical technique to solve eqn (12) is given in Gupta (1973).

Asymptotic analysis

The asymptotic analysis of the integral eqn (12) for a crack located in a homogeneous material, with its tip impinging on a nonhomogeneous material, has already been done by Kaw *et al.* (1992). Their investigation verified that the singularity in the slope function is of the type $G(t) = H(t)/(a^2-t^2)^{\gamma}$. The power of the singularity, γ is identical to the case of the crack impinging on a homogeneous material with properties which are the same as those of the nonhomogeneous material at the interface. The value of the power of the singularity, γ, is given by the root $(0 < \gamma < 1)$ of the characteristic equation

$$2\cos\pi\gamma + 4\lambda_2(\gamma-1)^2 - (\lambda_1+\lambda_2) = 0. \tag{13}$$

In eqn (13), λ_1 and λ_2 are functions of the elastic properties of the materials on either side of the interface that the crack tip is embedded in and are given by

$$\lambda_1 = \frac{\kappa_1\mu_2 - \kappa_2\mu_1}{\mu_2+\kappa_2\mu_1}, \qquad \lambda_2 = \frac{\mu_2-\mu_1}{\mu_1+\kappa_1\mu_2}, \tag{14a, b}$$

where μ_1 and μ_2 are the shear moduli of strips 1 and 2 at the interface, respectively, and ν_1 and ν_2 are the Poisson's ratios of strips 1 and 2 at the interface, respectively, and

$$\kappa_i = \frac{(3-\nu_i)}{(1+\nu_i)} \quad \text{(plane stress)}, \tag{15a}$$

$$\kappa_i = 3-4\nu_i \quad \text{(plane strain)}. \tag{15b}$$

Stress intensity factor and stresses

The stress intensity factor at the crack tip is calculated as

$$\begin{aligned} K &= \lim_{x_1\to a^+} \sqrt{2}(x_1-a)^{1/2}\sigma_{yy}^1(x_1,0), \quad \text{if} \quad a < h_1, \\ &= \lim_{x_2\to 0^+} \sqrt{2}x_2^{\gamma}\sigma_{yy}^2(x_2,0), \quad \text{if} \quad a = h_1, \end{aligned} \tag{16}$$

where σ_{yy} is the normal stress in front of the crack tip. The stress intensity factor is then expressed in terms of the numerical solution variables as

$$K = -2\sqrt{2}\mu^*\left(\frac{a}{2}\right)^{\gamma}\psi(1), \tag{17}$$

where

$$\psi(1) = \lim_{t\to a^-}\frac{G(t)(a^2-t^2)^{\gamma}}{a^{2\gamma}}, \tag{18}$$

and

$$\mu^* = \frac{2\mu_1}{1+\kappa_1}, \quad a < h_1,$$

$$= \frac{\mu_1\mu_2}{\sin(\pi\gamma)}\left[\frac{1+2\lambda_1(1-\gamma)}{\mu_1+\kappa_1\mu_2} + \frac{1-2\lambda_2(1-\gamma)}{\mu_2+\kappa_2\mu_1}\right], \quad a = h_1. \tag{19}$$

The stresses are calculated by solving eqn (12) numerically and substituting the unknown functions in the stress field [eqns (2a–c) and (4a–c)].

Definition of models

As discussed in the introduction, four families of composite fracture problems are solved.

Model 1 : *composites with nonhomogeneous interphases*

The geometry for this model is shown in Fig. 2. A cracked fiber layer is attached through a nonhomogeneous interphase of width h_2 to a homogeneous matrix layer of width $h_m \gg h_f$.

The Young's modulus, $E_2(x_2)$ and the Poisson's ratio, $\nu_2(x_2)$ of the interphase can vary arbitrarily through the width of the interphase, h_2. This is made possible by approximating the given elastic moduli variation in the interphase by piecewise continuous exponentially varying splines. Geometrically, the interphase strip is divided into "q" substrips. In each substrip "j", $j = 1, 2, \ldots, q$, the elastic moduli varies exponentially through its width $(h_2^{j+1} - h_2^j)$ as

$$E_2^j(x_2) = E_0^j\, e^{\beta_j x_2}, h_2^j < x_2 < h_2^{j+1}, \quad j = 1, 2, \ldots, q, \tag{20a}$$

$$\nu_2^j(x_2) = (a_0^j + b_0^j x_2)\, e^{\beta_j x_2}, \quad h_2^j < x_2 < h_2^{j+1}, \quad j = 1, 2, \ldots, q, \tag{20b}$$

$$h_2^1 = 0 \tag{20c}$$

$$h_2^{q+1} = h_2. \tag{20d}$$

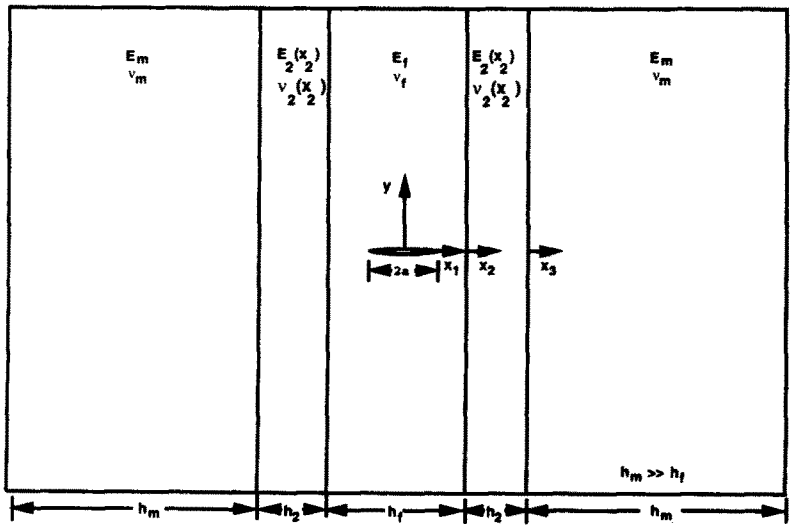

Fig. 2. Geometry of a composite with a nonhomogeneous interphase.

The width $(h_2^{j+1}-h_2^j)$ and the number of the substrips (q) needed are found iteratively until the relative difference between the elastic moduli of the interphase, $E_2(x_2)$ and $v_2(x_2)$, and the evaluated exponential splines, $E_2^j(x_2)$ and $v_2^j(x_2)$, are within a prespecified tolerance. A tolerance of 1% was used in this study. If the interphase is a multicomponent phase (Drzal, 1983) of chemically distinct phases, each component of the interphase is approximated by a separate homogeneous layer.

The interphase elastic properties are approximated by exponentially varying splines through its width because derivation of exact displacement and stress fields in Fourier transforms are only possible for exponential variations (Delale and Erdogan, 1988). Moreover, these displacement and stress fields were found possible only for plane stress conditions. This is also the only reason for choosing plane stress conditions for the whole composite geometry for Model 1.

A continuous variation of the elastic moduli was assumed through the interphase width for this study, but is not necessary. The discontinuities in the Young's modulus and the Poisson's ratio in the interphase could be included. Assuming continuity at the strip interfaces gives

$$\beta_j = \log\left[\frac{E_2^j(h_2^{j+1})}{E_2^j(h_2^j)}\right]\Big/(h_2^{j+1}-h_2^j), \tag{21a}$$

$$E_0^j = E_2^j(h_2^j), \tag{21b}$$

$$b_0^j = [v_2(h_2^{j+1})\,e^{\beta_j(h_2^{j+1}-h_2^j)} - v_2(h_2^j)]/(h_2^{j+1}-h_2^j), \tag{21c}$$

$$a_0^j = v_2(h_2^j), \quad j = i, 2, \ldots, q. \tag{21d}$$

The elastic moduli of the interphase are assumed to vary quadratically ($Q1$, $Q2$, $Q3$, $Q4$) or linearly along is width. The elastic moduli are assumed to be continuous at the fiber interphase and the interphase–matrix interfaces for all of the interphase substrips. The linear variations of the interphase properties is shown to be approximated by substrips with exponentially varying properties in Fig. 3(a). Figure 3(b) shows the four quadratic variations of the Young's modulus in an interphase strip. The slope of the interphase elastic properties with respect to the width is zero in $Q1$ at the fiber–interphase interface and is zero in $Q4$ at the interphase–matrix interface. The variation $Q2$ lies between the cases of linear variation and $Q1$, and the variation $Q3$ lies between the cases of the linear variation and $Q4$. Applying these conditions yields

$$\text{Linear:} \quad E_2(x_2) = \left(\frac{E_m - E_f}{h_2}\right)x_2 + E_f, \tag{22a}$$

$$Q1: \quad E_2(x_2) = \left(\frac{E_m - E_f}{h_2^2}\right)x_2^2 + E_f, \tag{22b}$$

$$Q2: \quad E_2(x_2) = \left(\frac{E_m - E_f}{2h_2^2}\right)x_2^2 + \left(\frac{E_m - E_f}{2h_2}\right)x_2 + E_f, \tag{22c}$$

$$Q3: \quad E_2(x_2) = -\left(\frac{E_m - E_f}{2h_2^2}\right)x_2^2 + 3\left(\frac{E_m - E_f}{2h_2}\right)x_2 + E_f, \tag{22d}$$

$$Q4: \quad E_2(x_2) = -\left(\frac{E_m - E_f}{h_2^2}\right)x_2^2 + 2\left(\frac{E_m - E_f}{h_2}\right)x_2 + E_f, \tag{22e}$$

where E_f and E_m are the fiber and the matrix Young's moduli, respectively. In eqns (22a–e), x_2 is the horizontal distance from the cracked layer–interphase interface.

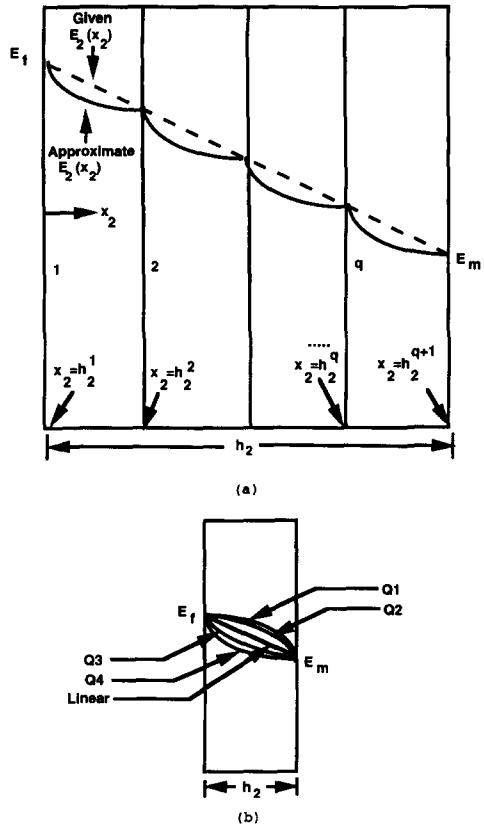

Fig. 3(a) Dividing the nonhomogeneous interphase into equivalent strips with exponentially varying elastic moduli; (b) variations of interphase elastic moduli.

Model 2: composites with nondilute fiber volume fraction

Figure 4 shows a cracked layer bonded to several alternating layers of the matrix and the fiber. Plane strain is assumed. This model investigates the effects of the nondilute fiber volume fraction on the fracture mechanics of composites. The global fiber volume fraction, V_{fg}, is calculated as

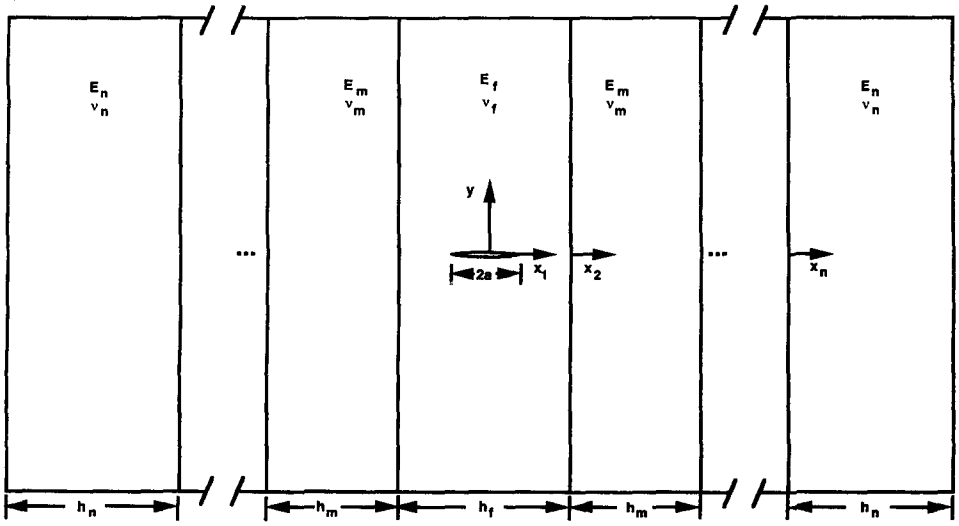

Fig. 4. Geometry of a composite with a nondilute fiber volume fraction.

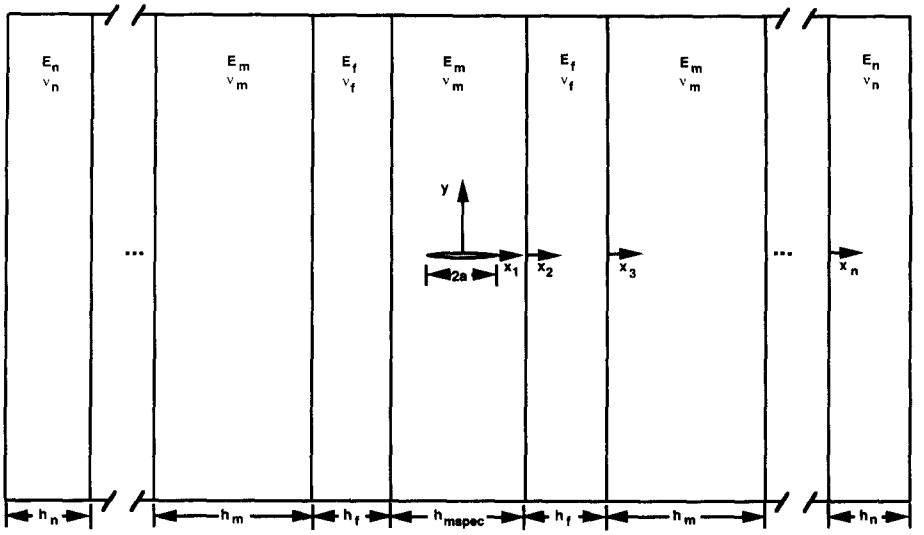

Fig. 5. Geometry of a composite with irregular fiber spacing.

$$V_{fg} = h_f/(h_m + h_f), \tag{23}$$

where h_m and h_f are the matrix layer and the fiber layer widths, respectively. All the fiber layers are of equal width, h_f and all the matrix layers are also of equal width, h_m. This simulates a uniform arrangement of the fibers in the composite.

Model 3 : *composites with irregular fiber spacing*

An arrangement similar to the one in Model 2 is used to model the effect of the nonuniformly spaced fibers (Fig. 5). A cracked matrix layer of width h_{mspec} is bonded to alternating fiber and matrix layers of width h_f and h_m, respectively. The local fiber volume fraction, V_{fl}, is calculated based on the cracked matrix layer width as

$$V_{fl} = h_f/(h_{mspec} + h_f). \tag{24}$$

The global fiber volume fraction is calculated based on the width of the undamaged matrix layer using eqn (23). This simulates two fibers placed closer to, or further from, each other than the average distance between the fibers. All other fibers are spaced uniformly.

Model 4 : *hybrid composites*

Figure 6 shows the model with more than one type of fiber. A hybrid composite is simulated here by alternating high and low stiffness fiber layers. The stiffer fibers are referred to as the original fibers, and the less stiff fibers as the hybrid fibers. The same width, h_f is assumed for all the fiber layers and the same width, h_m is assumed for the matrix layers. Therefore, a combined fiber volume fraction including fibers of both types is calculated using eqn (23).

DISCUSSION OF RESULTS

The following checks were made to verify the numerical results of this study. All boundary and continuity conditions were found to be satisfied. Also, the stress intensity factors (SIF) at the crack tips and the stresses were checked with the special cases available in the literature. These include the Griffith crack problem (Sneddon, 1951), the problem of a cracked layer between two homogeneous half-planes (Gupta, 1973), and the problem of a cracked layer bonded to two homogeneous half-planes through a nonhomogeneous interphase (Kaw *et al.*, 1992).

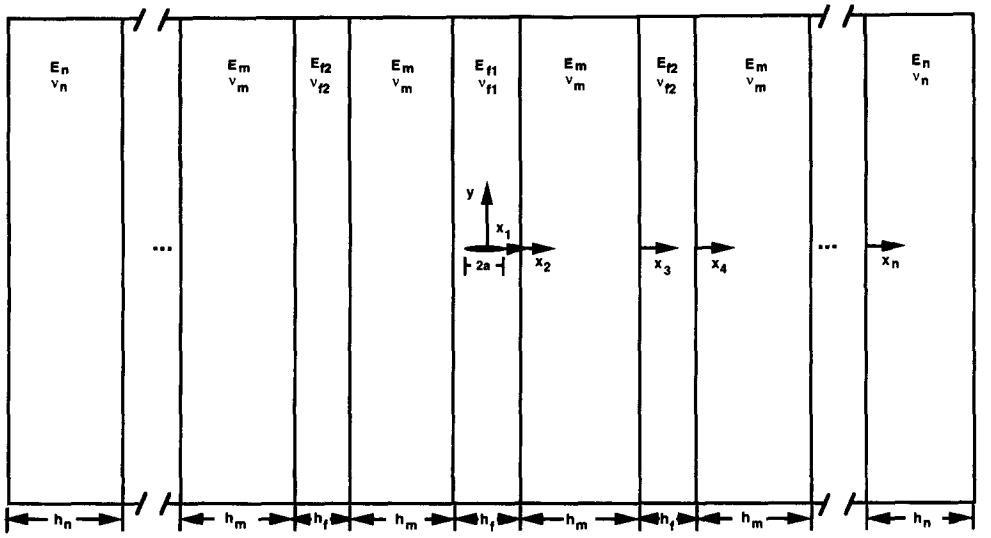

Fig. 6. Geometry of a hybrid composite.

For all the models except Model 3, the fiber and the matrix Poisson's ratio throughout the study is taken equal to 0.3 and the crack is assumed to be up to the interface, $a = h_1$. Also, all the models, except Model 1, are solved with plane strain assumptions.

Model 1 : *composites with nonhomogeneous interphases*

Figure 7 shows the normalized SIF as a function of the fiber to matrix moduli ratio, E_f/E_m for five types of nonhomogeneous interphases and for a crack touching the interface ($a = h_1$).

In Fig. 7, the SIF was normalized by the SIF for the interphase with the linear variation of elastic properties. The plot for the linear interphase case is, hence, a constant line. A range of $1/3 < E_f/E_m < 3$ is chosen. Cases outside the above E_f/E_m range required prohibitive computational times. However, a difference of as much as 14% was found between the normalized SIF for the $Q1$ and $Q4$ variations for a range of $1/3 < E_f/E_m < 3$. The effects

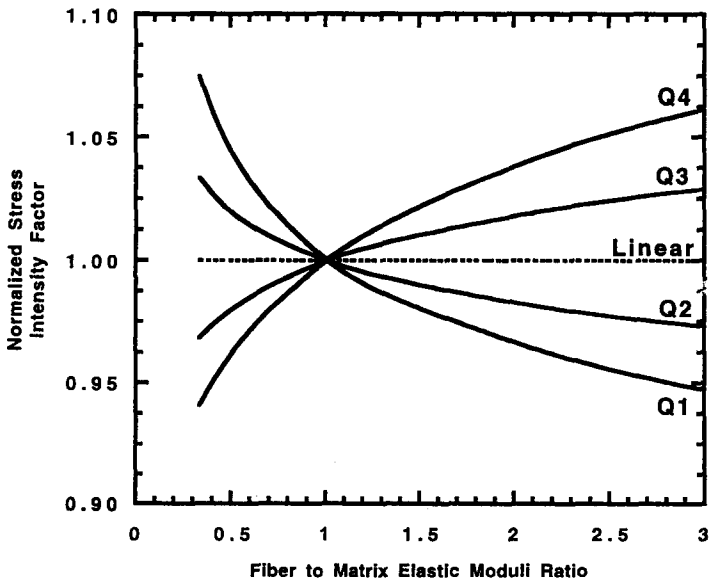

Fig. 7. Normalized stress intensity factor as a function of fiber to matrix elastic moduli ratio for nonhomogeneous interphase cases (Model 1, $a/h_1 = 1$, $V_f \ll 1$).

of varying properties in the interphase would be magnified for typical advanced polymer matrix composites where the ratio E_f/E_m is as high as 80/1.

In Fig. 7, the normalized SIF was lower for $Q1$ than for the other four variations when $E_f/E_m > 1$. To understand this, an average Young's modulus, E_{ave} was found near the crack tip over a distance of +10% of the interphase width starting at the crack tip as

$$E_{ave} = \frac{1}{0.1h_2} \int_0^{(0.1h_2)} E_2(x_2)\, dx_2. \tag{25}$$

This calculation for the cases of $E_f/E_m > 1$ gives the order,

$$(E_{ave})_{Q1} > (E_{ave})_{Q2} > (E_{ave})_{linear} > (E_{ave})_{Q3} > (E_{ave})_{Q4}$$

and vice versa for $E_f/E_m < 1$. Therefore, for cases where $E_f/E_m > 1$, the crack tip is embedded in a region of higher average elastic moduli for $Q1$, which locally carries more load and relieves the stress concentration at the crack tip. The relative average crack tip elastic moduli theory also explains why the graph inverts for $E_f/E_m < 1$.

The same graph shows that for $E_f/E_m > 1$, the normalized SIF increases for the $Q3$ and $Q4$ cases and decreases for the $Q2$ and $Q1$ cases as a function of E_f/E_m. The plot is then inverted for $E_f/E_m < 1$. This is again explained by the concentration of stiffer material near the crack tip.

Model 2: composites with nondilute fiber volume fraction

A study was done first to determine how many strips were required for convergent results for the composite geometry with a nondilute fiber volume fraction. The extreme case of $V_f = 0.5$ and $E_f/E_m = 1/20$ was used. The axial (σ_{yy}) and transverse (σ_{xx}) stresses at $x_2/h_1 = y/h_1 = 1.0$ normalized by the crack pressure, and the SIF normalized by ($p\sqrt{a}$) changed negligibly for more than seven total ($n = 4$) layers (Figs 8 and 9).

The normalized SIF is plotted as a function of the global V_f in Fig. 10 for cracks up to the interface ($a = h_1$). The SIF was normalized by the SIF for the same E_f/E_m ratio for Gupta's (1973) model ($V_f = 0$). This normalization isolates the effect of the V_f on the SIF. In all cases, E_f/E_m was calculated based on the cracked layer being the fiber layer.

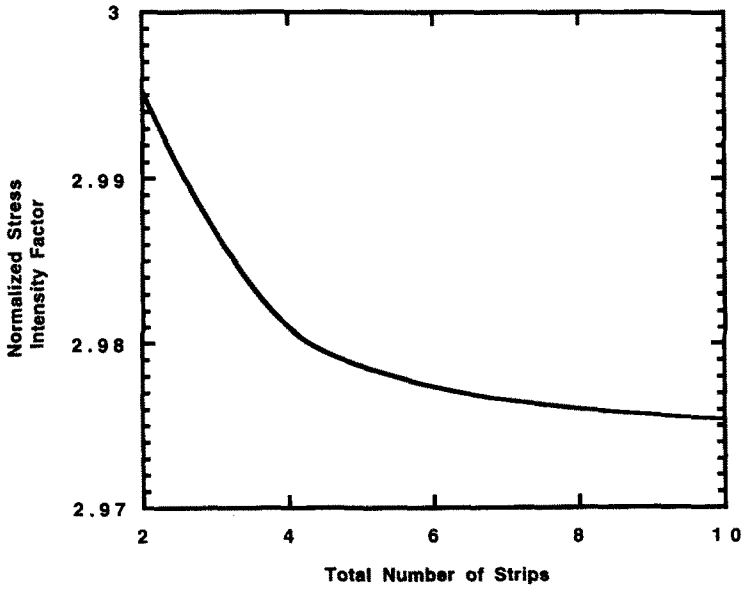

Fig. 8. Normalized stress intensity factor as a function of number of strips (Model 2, $E_f/E_m = 1/20$, $a/h_1 = 1$, $V_f = 0.5$).

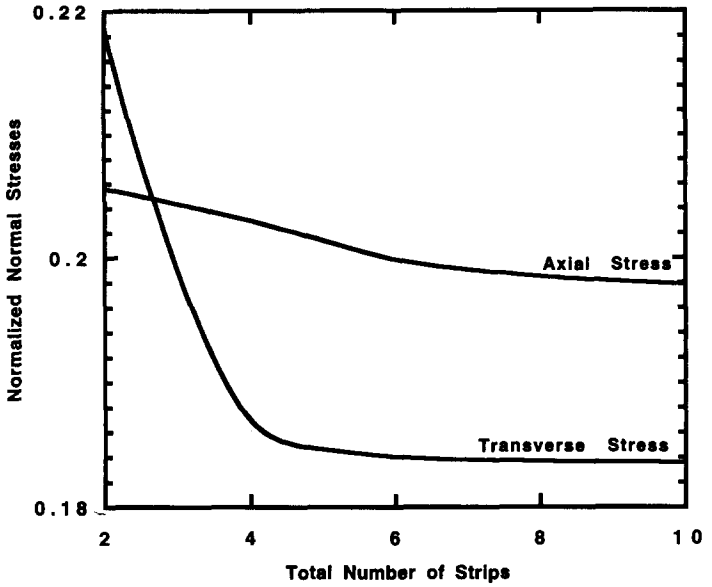

Fig. 9. Normalized stresses as a function of number of strips (Model 2, $E_f/E_m = 1/20$, $a/h_1 = 1$, $V_f = 0.5$).

In Fig. 10, the normalized SIF decreases about linearly with the increasing V_f and E_f/E_m for $E_f/E_m > 1$. These results are expected since a stiff fiber layer next to the damaged fiber layer is located closer for increasing V_f. However, for $E_f/E_m < 1$, the decrease in the normalized SIF with an increase in V_f is negligible. For example, only a difference of 1% was observed between the range of $0 < V_f < 0.5$ for a typical $E_f/E_m = 1/6$.

The average axial stress $y/h_1 = 1$ is plotted as a function of the global V_f for constant E_f/E_m in Fig. 11. The average axial stress at $y/h_1 = 1$ across the cracked layer normalized by the crack pressure is a measure of the load diffusion in the cracked layer. The average axial stress values increased by as much as 12% for $E_f/E_m = 12/1$ when increasing the V_f from zero to one half. The average axial stress increases with an increase in E_f/E_m for $E_f/E_m > 1$ and vice versa.

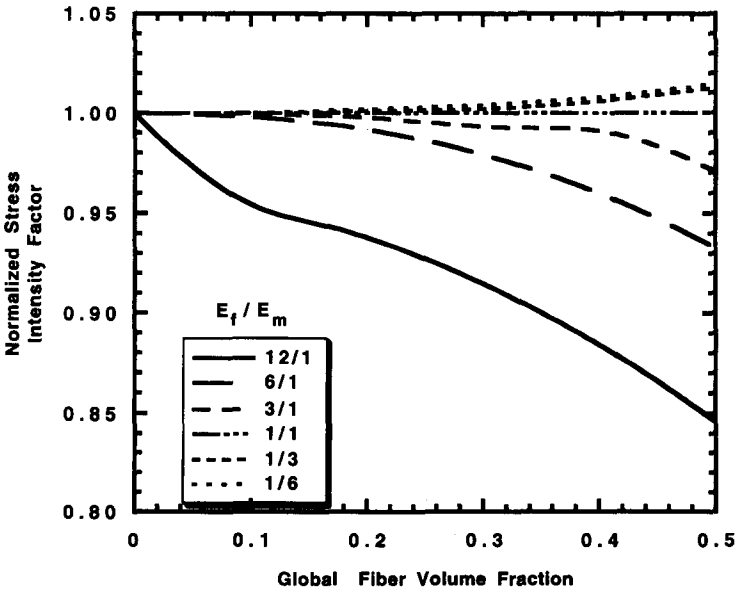

Fig. 10. Normalized stress intensity factor as a function of global fiber volume fraction for constant fiber to matrix elastic moduli ratio (Model 2, $a/h_1 = 1$).

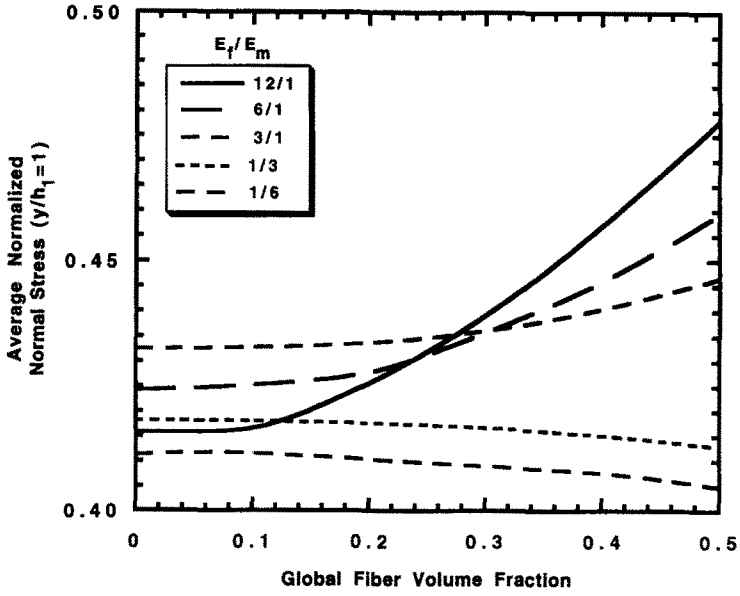

Fig. 11. Average normalized normal stress as a function of global fiber volume fraction for constant fiber to matrix elastic moduli ratio (Model 2, $a/h_1 = 1$).

The present model was also used to understand the crack deflection criteria for composites. A transverse crack at a fiber–matrix interface can either transversely penetrate the adjacent medium or grow along the interface. The determination of the crack path is an indication of the failure mechanism in a composite and a measure of its fracture toughness.

The determination of the crack path is made as follows in the present study. Following Swenson and Rao (1970), the normalized peel stress (NPS) and the normalized shear stress (NSS) at the crack tip ($a = h_1$) are calculated as follows

$$\text{NPS} = \frac{\sigma_{xx}^2(0,0+)}{\sigma_{yy}^2(0+,0)}, \tag{26}$$

$$\text{NSS} = \frac{\sigma_{xy}^2(0,0+)}{\sigma_{yy}^2(0+,0)}. \tag{27}$$

Note that the stresses in the numerator and the denominator in eqns (26) and (27) are unbounded. Hence, the stresses are first numerically calculated near the crack tip along the interface for the peel [numerator of eqn (26)] and the shear stresses [numerator of eqn (27)], and along the crack plane for axial stresses [denominator of eqns (26) and (27)]. Then these stresses are used in the interpolation curve (Cook and Erdogan, 1972)

$$\sigma = C_1 r^{-\gamma} + C_2 r^{1-\gamma} + C_3 r^{2-\gamma} \tag{28}$$

to give the three stresses of eqns (26) and (27) at the crack tip, where r is the distance from the crack tip and γ is the order of the singularity of the stresses given by eqn (13). The ratios NPS and NSS, which are bounded, can now be calculated using eqns (26) and (27).

A crack deflection criteria is defined by Cornie *et al.* (1991). They report that if NPS (NSS) is greater than the ratio of the normal (shear) strength of the interface to the normal strength of the uncracked matrix, then the crack is assumed to debond along the interface. Otherwise, the crack is assumed to penetrate the matrix.

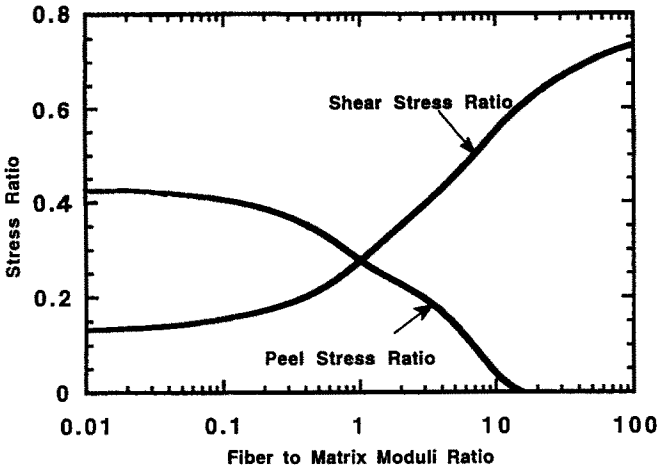

Fig. 12. Normalized interfacial peel and shear stresses at the crack tip as a function of fiber to matrix elastic moduli ratio for constant global fiber volume fraction (Model 2, $a/h_1 = 1$, $V_f = 0.5$).

The NPS and NSS at the crack tip are plotted as a function of E_f/E_m for constant global V_f in Fig. 12. As E_f/E_m increases, NSS at the crack tip increases while NPS at the crack tip decreases. This implies that the interfacial bond at the crack tip is more likely to fail in a shear mode than in an opening mode as E_f/E_m increases. Also, these stress ratios were found to be independent of V_f. Hence the crack deflection criteria is dependent only on the relative elastic moduli of the fiber and the matrix. These conclusions are confirmed by Cornie *et al.* (1991) and He and Hutchinson (1989).

Model 3: *composites with irregular fiber spacing*

The composites with irregular fiber spacing problem was solved for the composite system considered by Wang *et al.* (1992). They considered the carbon/borosilicates system ($E_f = 380$ GPa, $v_f = 0.26$, $E_m = 63$ GPa, $v_m = 0.3$).

The effects on the SIF having uniformly spaced layers in the composite model are shown in Fig. 13 for the carbon/borosilicates system. The normalized SIF as a function of

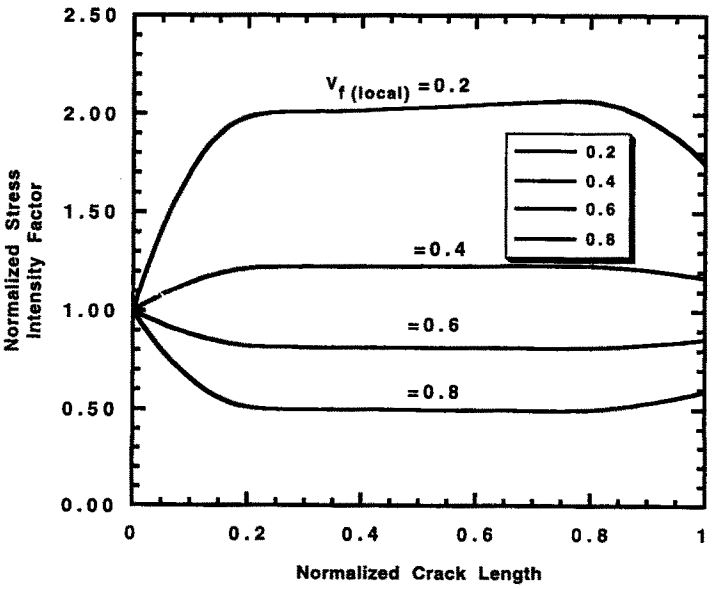

Fig. 13. Normalized stress intensity factor as a function of normalized crack length for constant local fiber volume fraction (Model 3, $V_{fg} = 0.5$, $E_f/E_m = 380/63$).

the normalized crack length, a/h_1 for constant global V_f are plotted. The SIF is normalized by the SIF for the case of uniform spacing for the same normalized crack lengths. This isolates the effect of the local fiber spacing.

The global fiber volume fraction used was 0.5. Hence, the no defect case is a local fiber volume fraction of 0.5. The local fiber volume fraction was calculated from eqn (24) and is a measure of how much the width of the cracked matrix layer differs from the width of the other uniformly spaced matrix layers.

The normalized SIFs are nearly independent of the normalized crack length except near the extremes of a very small crack and a crack approaching the interface. As expected, for crack lengths approaching zero, the normalized SIF approaches one (Griffith crack problem). As the crack tip approached the fiber–matrix interface, the normalizd SIF increased for a local $V_f < 0.5$. and decreased for a local $V_f > 0.5$.

Therefore, a crack in a matrix region between two fibers placed farther apart than the other fibers is more likely to grow that the crack located in a matrix region between two fibers uniformly spaced. If it is assumed that microcracks pre-exist in the matrix and a matrix crack is initiated when the microcracks begin to grow, then the matrix crack initiation stress (MCIS) is lower in a region of low local V_f.

Figure 13 also indicates that a matrix crack is less likely to develop and grow between fibers that are placed closer together. This correlates with trends in the experimental data from Barsoum *et al.* 1992). Preliminary results from Barsoum *et al.* (1992) showed that the MCIS was approximately halved when the local fiber spacing doubled. In Fig. 13, the normalized SIF doubled between a local V_f of 0.4 and 0.2 which corresponds to doubling the local fiber spacing. This observation is made for the constant portion of the curves for a normalized crack length between 0.2 and 0.8. Since the MCIS is assumed to be inversely proportional to the stress intensity factor, the analytical results track their experimental results. Conversely, for a composite loaded transversely, Xu *et al.* (1992) concluded that the most likely crack path is not between the fibers placed far apart, but between the fibers placed close to each other. Hence, the uniform placement of fibers is critical in the manufacturing of high fracture toughness composites used under complex loading.

Model 4: *hybrid composites*

Figure 6 shows the arrangement of the fiber and the matrix layers for the hybrid composite problem. The cracked fiber and every other fiber layer after that are of the original stiffer fiber type. The second fiber layer and every other fiber layer after that are the less stiff hybrid fiber layers. The widths of the two fiber types are equal. Figure 14 shows

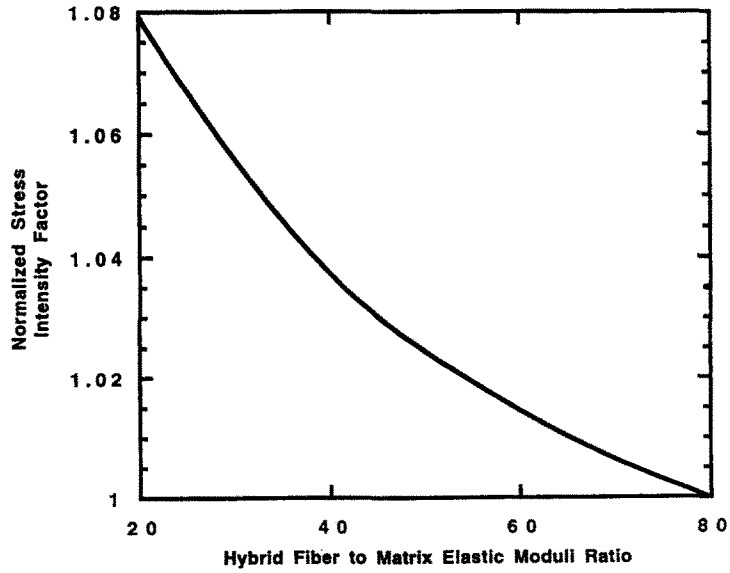

Fig. 14. Normalized stress intensity factor as a function of hybrid fiber to matrix elastic moduli ratio (Model 4, $E_{f(original)}/E_m = 80$, $a/h_1 = 1$, $V_f = 0.5$).

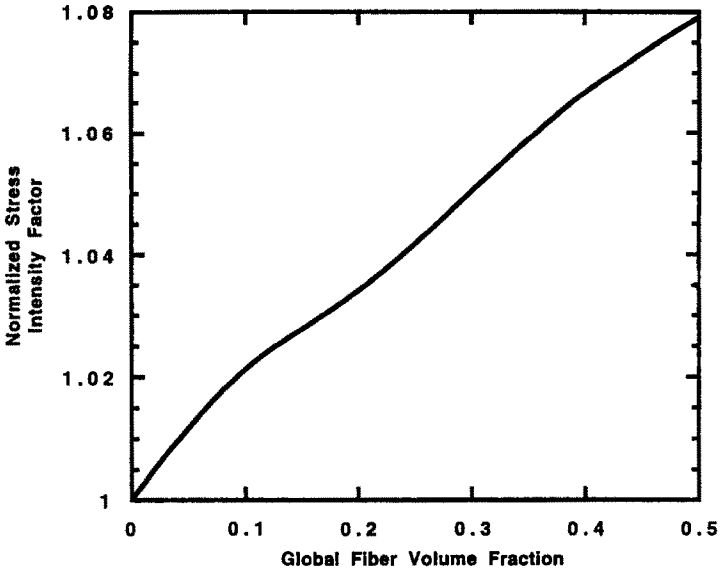

Fig. 15. Normalized stress intensity factor as a function of global fiber volume fraction (Model 4, $E_{f(original)}/E_m = 80$, $E_{f(hybrid)}/E_m = 20$, $a/h_1 = 1$).

a graph of the normalized SIF as a function of the hybrid E_f/E_m for constant V_f for $a/h_1 = 1$. The combined fiber volume fraction was taken as 0.5. A range of $E_f/E_m = 20/1$ (glass/epoxy) to 80/1 (graphite/epoxy) was used. The value of E_f/E_m for the original fiber layers was taken as 80/1. The SIF was normalized by the SIF for the non-hybrid case where all the fiber layers have $E_f/E_m = 80/1$.

Figure 14 shows that the normalized SIF increases linearly with a decrease in the hybrid fiber elastic moduli. This corresponds to a drop in the elastic moduli of the second fiber layer which then is carrying less load.

The normalized SIF as a function of the V_f (combined volume fraction of both fiber constituents) for constant E_f/E_m ratio is shown in Fig. 15. The value of E_f/E_m for the original fibers and the hybrid fibers is again assumed as 80/1 and 20/1, respectively. The SIF is normalized by the SIF for the nonhybrid case (all fiber layers having $E_f/E_m = 80/1$) of the corresponding V_f. The normalized SIF increases linearly with increasing V_f. These results indicate that the effect of replacing some original fibers with less stiff hybrid fibers is more significant at higher fiber volume fractions.

CONCLUSIONS

The following conclusions are made about the initially damaged, layered composite model under a remote axial strain studied in this work.

1. The fibers and the matrix layers away from the damaged layer affect the critical stresses and the stress intensity factor at the crack tip. However, the ratios of the stresses at the crack tip, which determine crack deflection, are dependent only on the relative properties of the damaged and the adjacent medium, and are independent of the geometry and the material properties away from the crack tip.

2. A crack is less likely to grow into a nonhomogeneous interphase that has a greater average elastic moduli near the cracked layer–interphase interface.

3. The stress intensity factor decreases linearly with an increase in the fiber volume fraction if the fiber is stiffer than the matrix. This decrease becomes higher as the fiber to matrix moduli ratio increases. For a typical fiber volume fraction of 0.5, this decrease is about 1% per unit increase in the fiber to matrix moduli ratio. However, if the damaged fiber layer is more compliant than the matrix, the fiber volume fraction has a negligible effect on the stress intensity factor.

4. For a cracked fiber, as the fiber to the matrix elastic moduli ratio increases, the mode of the interface failure is more likely to be the shear mode than the opening mode, assuming that the matrix and the interfacial strengths are constant for all cases.

5. The matrix crack initiation stress is inversely proportional to the local fiber spacing.

6. For typical hybrid polymer composites, where half of the high elastic moduli fibers are replaced by low elastic moduli fibers, the stress intensity factor at the crack tips may increase only by as much as 10%.

Acknowledgements—This work was supported by AFOSR, Bolling AFB, Washington DC, via Grant F49620-92-J-0542. The first author also acknowledges the support of the 1992 AFOSR/RDL Graduate Student Summer Research Program and the 1991–92 USF Graduate Fellowship Program. The technical discussions with Dr N. J. Pagano of WPAFB, Ohio and the encouragement of the AFOSR grant monitor, Dr W. F. Jones are deeply appreciated.

REFERENCES

Agarwal, B. D. and Broutman, L. J. (1991). *Analysis and performance of fiber composites*, pp. 230–234. Wiley, New York.

Barsoum, M. W., Kangutkar, P. and Wang, A. S. D. (1992). Matrix crack initiation in ceramic matrix composites part I: experiments and test results. *Compos. Sci. Tech.* **44,** 247–269.

Brennan, J. J. (1987). Interfacial chemistry and bonding in fiber reinforced and glass–ceramic matrix composites. In *Ceramic Microstructures '86: Role of Interfaces* (Edited by J. A. Park and A. G. Evans), pp. 387–399. Plenum, New York.

Chamis, C. C. (1974). Mechanics of load transfer at the interface. *J. Compos. Mater.* **6,** 32–77.

Cook, T. S. and Erdogan, F. (1972). Stresses in bonded materials with a crack perpendicular to the interface. *Int. J. Engng Sci.* **10,** 677–697.

Cornie, A., Argon, A. S. and Gupta, V. (1991). Designing interfaces in inorganic matrix composites. *MRS Bulletin* **16,** 32–38.

Delale, F. and Erdogan, F. (1988). On the mechanical modeling of the interfacial region in bonded half-planes. *ASME J. Appl. Mech.* **55,** 317–324.

Drzal, L. T. (1983). Composite interphase characterization. *SAMPE J.* **19,** 7–13.

Drzal, L. T. (1986). The interphase in epoxy composites. *Adv. Polymer Sci.* **75,** 1–32.

Erdogan, F. and Bakioglu, M. (1976). Fracture of plates which consist of periodic dissimilar strips. *Int. J. Fract. Mech.* **12,** 71–84.

Erdogan, F., Kaya, A. C. and Joseph, P. (1991). The crack problem in nonhomogeneous materials. *ASME J. Appl. Mech.* **58,** 410–418.

Gupta, G. D. (1973). A layered composite with a broken laminate. *Int. J. Solids Structures* **9,** 1141–1154.

He, M. Y. and Hutchinson, J. W. (1989). Crack deflection at an interface between dissimilar elastic materials. *Int. J. Solids Structures* **9,** 1053–1067.

Jayaram, K., Reifsnider, K. L. and Swain, R. E. (1993a). Elastic and thermal effects in the interphase: part I comments on characterization methods. *ASTM J. Comp. Tech. Res.* **15,** 3–13.

Jayaram, K., Reifsnider, K. L. and Swain, R. E. (1993b). Elastic and thermal effects in the interphase: part II comments on modeling studies. *ASTM J. Comp. Tech. Res.* **15,** 14–22.

Kaw, A. K., Selvarathinam, A. S. and Besterfield, G. H. (1992). Comparison of interphase models in a fracture problem in fiber reinforced composites. *J. Theoret. Appl. Mech.* **17,** 133–147.

Mori, T. and Tanaka, K. (1973). Average stress in matrix and average elastic energy of materials with misfitting inclusions. *Acta Metall.* **21,** 571–574.

Pagano, N. J. and Brown, H. W. (1993). The full-cell cracking mode in unidirectional brittle matrix composites. *Composites* **24,** 69–83.

Sneddon, I. N. (1951). *Fourier Transforms*. McGraw-Hill, New York.

Sottos, N. R., McCullough, R. L. and Scott, W. R. (1992). The influence of interphase regions on local thermal displacements in composites. *Compos. Sci. Tech.* **43,** 1–14.

Summerscales, J. and Short, D. (1978). Carbon fibre and glass fibre hybrid reinforced plastics. *Composites* **9,** 157–166.

Swenson, D. O. and Rau, C. A. (1970). The stress distribution around a crack perpendicular to an interface between materials. *Int. J. Fract. Mech.* **6,** 357–365.

Wang, A. S. D., Huang, X. G. and Barsoum, M. W. (1992). Matrix crack initiation in ceramic matrix composites part II: models and simulation results. *Compos. Sci. Tech.* **44,** 271–282.

Whitney, J. M. and Brown, H. W. (1993). Approximate stress analysis of a unidirectional composite containing a broken fiber. *Proceedings of the Sixth Japan–US Conference on Composite Materials*, pp. 500–510. Technomic, Orlando.

Xu, Y. L., Delale, F. and Liaw, B. M. (1992). Effect of temperature and fiber distribution on matrix cracking in ceramic matrix composites. *Comp. Engng* **2,** 67–79.